Chemical Physics Letters 679 (2017) 6–14

Contents lists available at ScienceDirect

Chemical Physics Letters

journal homepage: www.elsevier.com/locate/cplett

Research paper

Multiscale simulation on shearing transitions of thin-film lubrication with multi-layer molecules

Z.-B. Wu [a,b,*], X.C. Zeng [c]

[a] State Key Laboratory of Nonlinear Mechanics (LNM), Institute of Mechanics, Chinese Academy of Sciences, Beijing 100190, China
[b] School of Engineering Science, University of Chinese Academy of Sciences, Beijing 100049, China
[c] Department of Chemistry, University of Nebraska-Lincoln, Lincoln, NE 68588, USA

ARTICLE INFO

Article history:
Received 24 February 2017
In final form 23 April 2017
Available online 25 April 2017

Keywords:
Thin-film lubrication
Coarse-graining model
Shear transitions
Tribology

ABSTRACT

Shearing transitions of multi-layer molecularly thin-film lubrication systems in variations of the film-substrate coupling strength and the load are studied by using a multiscale method. Three kinds of the interlayer slips found in decreasing the coupling strength are in qualitative agreement with experimental results. Although tribological behaviors are almost insensitive to the smaller coupling strength, they and the effective film thickness are enlarged more and more as the larger one increases. When the load increases, the tribological behaviors are similar to those in increasing coupling strength, but the effective film thickness is opposite.

1. Introduction

A thin fluid film confined between two solid substrates may prevent surfaces of the substrates coming into molecular contact and becoming damaged in the dry friction, which is termed as thin-film lubrication. The systematic friction force is reduced three orders of magnitudes when the dry friction is replaced by the thin-film lubrication. The thin-film lubrication is a very interesting topic on both fundamental theory and engineering application, such as viscous dampers, magnetic storage devices and designs of MEMS/NEMS [1–3]. A stick-slip phenomenon (the freezing-melting transition) appears in the molecularly thin film lubrication when the substrates are assumed as rigid. The critical friction force, which is quantized with the number of fluid molecular layers separating the surfaces, decreases as the number of fluid molecular layers increases [4–7]. For the thin film lubrication with multi-layer fluid molecules, the slipping process may have the partial and whole film melting due to the different interaction potentials between the solid and fluid molecules [8,9]. Although the surfaces of the substrates are smooth on macroscopic scale, they actually make molecular contact through the medium of the thin-film. In particular, the solid substrates may have multiple spatial scales and influence the microscopic motions of both the solid and fluid molecules near/within the film [10–12]. It is therefore necessary to include the details of molecular motions in the substrates to treat the shearing transitions of the thin-film lubrication with multi-layer fluid molecules. To fully understand the physical mechanism of the thin-film lubrication system, the heterostructure interface is described by an atomistic model, while the elastic behavior of the much thicker substrate is modeled by the finite element method. Such multiscale problem of the thin-film lubrication system must be reflected in a theoretical model.

During the past three decades a series of effective methods combining atomistic and continuum descriptions of fluids and solids are developed [13–35]. On the one hand, several effects on fluid flow near the walls have been made by applying the molecular dynamics to follow the trajectories of the fluid atoms in the layers near the walls and extend the non-sliding boundary conditions near the walls to the sliding ones. Beyond that the hydrodynamic equations are employed, the molecular dynamics and hydrodynamic treatments are self-consistently joined in the transition region that overlaps the two regimes of the atomistic and continuum descriptions. On the other hand, within the context of solid materials, two kinds of the effects to combine atomistic and continuum descriptions of the behaviors of materials have been completed at zero temperature. One is the FEAt procedure, where a core region described at the atomistic scale is surrounded by a transition region connected with the continuum regions covered by finite elements (FE). The other is a quasicontinuum treatment, where the whole lattices of material are overlayed with a FE mesh. The energy density in each FE is evaluated with the movements of its nodes. By including effects of thermal motions on the dynamics of certain processes, the FEAt and quasicontinuum methods are extended to finite temperature. Moreover, in a treatment of crack

* Corresponding author at: State Key Laboratory of Nonlinear Mechanics (LNM), Institute of Mechanics, Chinese Academy of Sciences, Beijing 100190, China.
E-mail address: wuzb@lnm.imech.ac.cn (Z.-B. Wu).

http://dx.doi.org/10.1016/j.cplett.2017.04.079
0009-2614/

propagation in pure silicon, to make a multiscale modeling approach that dynamically couples different length scales and accounts for thermal effects, the macroscopic atomistic ab-initial dynamics (MAAD) is developed. The molecular dynamics (MD) with the tight-binding approximation, the MD with the semi-empirical potential energy and the FE method are applied in the different length scales ranging from the atomic scale through the microscale and finally to the mesoscale/macroscale. In particular, the soft matter as a subfield of condensed matter comprising a variety of biological systems such as macromolecular assemblies has both fluid and solid properties. To investigate its long time- and length-scale behaviors, the multiscale approaches with quasi-equilibrium assumptions [36,37], the hybrid continuum method mixing the classical force field and coarse grained model [38,39] and the multiscale algorithm with the order parameters [40,41] have been developed. The multiscale analysis as a powerful methodology plays a critical role in the biological processes.

It is noted that for the thin-film lubrication system, the evolution of the system is slower than the molecular motions. In other words, on the time scale of the relevant process the system remains thermodynamic equilibrium. Such reversible or quasi-static processes of the thin-film lubrication can be described by means of Monte Carlo methods. In previous articles [42,43] we developed the multiscale description of fluid-solid interfacial systems and applied it to treat the monolayer film lubrication with elastic substrates. The far-region solid substrates are coarse-grained by local and non-local elements. The systematic free-energy related to the elements is corrected by the local harmonic approximation. The principal conclusion of papers is that the hybrid atomistic-coarse-graining (HACG) scheme yields the shear-stress profiles and the mean separation curves in good agreement with those in the fully atomistic description of the system over a wide variety of conditions. However, since the simulations were performed only for a monolayer molecularly film lubrication, an extension to multi-layer molecularly film lubrication systems and an investigation of microscopic structures during the shearing slips are the purpose of the present article. In particular, the tribological behaviors in the multi-layer molecularly film lubrication system not only depend on the elasticity of substrates, but also on the adhesion strength between the film and substrates and the cohesive strength of the film. It was shown that an optimal choice of the interaction within fluids relative to the interaction between the fluids and substrates may reduce the kinetic friction force of the system [44]. Therefore, it is important to investigate the effects of the adhesion strength between the film and substrates on the shearing transitions in the system when the cohesive strength of the film is fixed.

The paper is organized as follows. In Section 2, a short description of the coarse-graining model and the computational procedure is provided. The numerical results for two cases of three-layer and four-layer molecularly film lubrication are analyzed in Section 3. Finally, in Section 4, some conclusions and discussions are given.

2. Coarse-graining model and computational procedure

The idealized 2D contact consists of two identical hexagonal close-packed crystalline substrates separated by a multi-layer molecularly thin-film at an atomically flat interface, as shown schematically in Fig. 1. The top/bottom wall is taken to be rigid with the nearest-neighbor distance, i.e., the lattice constant a. The bottom wall remains stationary in the "laboratory" reference frame; the top wall can be translated in the x- and y- directions, but remains parallel with the bottom wall. The walls serve as handles by which the substrates can be manipulated. The lateral alignment of the walls is specified by the register α, which is defined by

$$x_i^t = x_i^b + \alpha a, \tag{1}$$

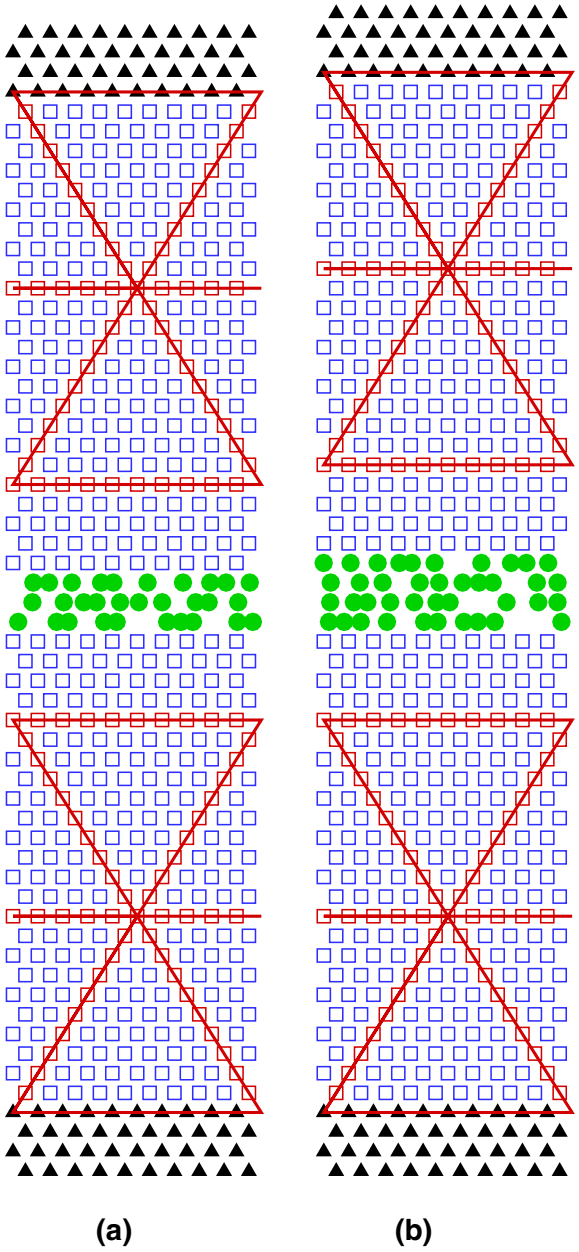

Fig. 1. Schematic of idealized two-dimensional contact with a thin fluid film for (a) three-layer atoms; (b) four-layer atoms and partial coarse-graining of far regions of substrates. Filled triangles, opened squares and filled circles represent solid atoms in the walls, solid atoms in substrates and fluid atoms in the film, respectively. All atoms are depicted in their initial configuration at $\alpha = 0$, where the atomistic positions in the film are random.

where x_i^t u and x_i^b denote the corresponding atomistic positions in the top and bottom walls, respectively. α is the fraction of the lattice constant by which the top wall is displaced laterally with respect to the bottom wall.

The tribological system only comprises the solid substrates plus the fluid film, but does not cover the walls. The solid substrates are divided into the near- and far-regions, which are depicted by using the atomistic and coarse-grained descriptions, respectively. The coarse-grained far regions of substrates are covered with a mesh of triangular elements. This coarse-graining partitions the original substrate atoms into two subsets: N_n nodal atoms and N_s non-nodal atoms. If one integrates the Boltzmann factor over the $2N_s$ degrees of freedom of the non-nodal atoms, one obtains an effective potential energy governing the motion of just the nodal atoms

$$V_{eff}(\mathbf{R}^{N_n}) = \sum_{e=1}^{N_e}(N_a^e \tilde{u}_e + N_s^e f_e), \tag{2}$$

where $\mathbf{R}^{N_n}$ stands for the nodal configuration, N_e for the number of elements, N_a^e the number of atoms underlying element e. The configurational energy per atom $\tilde{u}_e$ is expressed as

$$\tilde{u}_e = \frac{1}{2}\sum_{j\neq i} u_{ss}(r_{ij}), \tag{3}$$

where i denotes the "centroid" atom (i.e., the atom nearest the centroid of e) and j labels atoms that lie within the circle of radius r_c that is centered on i. The following shifted Lennard-Jones (12,6) potentials are taken as the pair interactions of the atoms

$$u_{ab} = \begin{cases} \phi_{ab}(r) - \phi_{ab}(r_c), & \text{if} \quad r < r_c; \\ 0, & \text{if} \quad r \geqslant r_c, \end{cases} \tag{4}$$

where

$$\phi_{ab}(r) = 4\epsilon_{ab}[(\sigma/r)^{12} - (\sigma/r)^6], \ ab = ff, fs, ss. \tag{5}$$

The effective diameter σ, ϵ_{ab} and range r_c is the same for all pairs. f_e is the Helmholtz energy per atom. By using the local harmonic approximation [45], f_e can be estimated as

$$f_e = 2k_BT \ln[h(\det D)^{1/4}/k_BT], \tag{6}$$

where the elements of the 2×2 dynamical matrix are given by $D_{kl} = m^{-1}(\partial^2 \tilde{u}_e/\partial x_k \partial x_l)_0 (k, l = 1, 2)$, k and l label Cartesian components $(x_1 = x, x_2 = y)$ of the position of the reference atom, and the subscript 0 signifies that the partial derivative is evaluated at the equilibrium configuration. To show the dynamic properties of molecularly thin-film lubrication, it was found that the numerical results based on the Lennard-Jones potentials are in qualitative agreement with the experimental ones [4].

The total configurational energy U_{cf} and the shear stress $T_{yx,cf}$ of the free-energy corrected HACG system are respectively given

$$\begin{aligned} U_{cf}(\mathbf{r}^{N_f}, \mathbf{r}^{N_s'}, \mathbf{R}^{N_n}) =& \frac{1}{2}\sum_{i=1}^{N_f}\sum_{j\neq i}^{N_f} u_{ff}(r_{ij}) + \sum_{i=1}^{N_f}\sum_{j=1}^{N_s'} u_{fs}(r_{ij}) \\ &+ \frac{1}{2}\sum_{i=1}^{N_s'}\sum_{j\neq i}^{N_s'} u_{ss}(r_{ij}) + \frac{1}{2}\sum_{i=1}^{N_s'}\sum_{j=1}^{N_s''} u_{ss}(r_{ij}) \\ &+ \frac{1}{2}\sum_{i=1}^{N_w}\sum_{j=1}^{N_s''} u_{ss}(r_{ij}) + \sum_{e=1}^{N_e} N_a^e\left[\frac{1}{2}\sum_{j\neq i} u_{ss}(r_{ij})\right] \\ &+ \sum_{e=1}^{N_e} N_s^e 2k_BT \ln[\hbar(\det D)^{1/4}/k_BT] \end{aligned} \tag{7}$$

and

$$\begin{aligned} T_{yx,cf} =& \frac{1}{2L_x}\sum_{i=1}^{N_f}\sum_{j\neq i}^{N_f} < u_{ff}'(r_{ij})x_{ij}y_{ij}/(r_{ij}L_y) > \\ &+ \frac{1}{L_x}\sum_{i=1}^{N_f}\sum_{j=1}^{N_s'} < u_{fs}'(r_{ij})x_{ij}y_{ij}/(r_{ij}L_y) > \\ &+ \frac{1}{2L_x}\sum_{i=1}^{N_s'}\sum_{j\neq i}^{N_s'} < u_{ss}'(r_{ij})x_{ij}y_{ij}/(r_{ij}L_y) > \\ &+ \frac{1}{2L_x}\sum_{i=1}^{N_s'}\sum_{j=1}^{N_s''} < u_{ss}'(r_{ij})x_{ij}y_{ij}/(r_{ij}L_y) > \\ &+ \frac{1}{2L_x}\sum_{i=1}^{N_w}\sum_{j=1}^{N_s''} < u_{ss}'(r_{ij})x_{ij}y_{ij}/(r_{ij}L_y) > \\ &+ \frac{1}{L_x}\sum_{e=1}^{N_e} N_a^e\left[\frac{1}{2}\sum_{j\neq i} < u_{ss}'(r_{ij})x_{ij}y_{ij}/(r_{ij}L_y) >\right] \\ &+ \frac{1}{L_x}\sum_{e=1}^{N_e} N_s^e\left[\frac{k_BT}{2} < \frac{1}{|D|}\frac{\partial|D|}{\partial\alpha a} >\right], \end{aligned} \tag{8}$$

where N_s' stands for the number of atoms in the near regions of the substrates, N_s'' for the number of underlying atoms in the far regions, N_e for the number of elements, N_a^e (N_s^e) the number of atoms (non-nodal atoms) underlying element e, k_B is Boltzmanns constant, $\hbar$ is Plancks constant and D is the local dynamical matrix associated with the centroid atom in a local element. The sliding with the register α is viewed as a quasistatic (or reversible) process. To compute the thermomechanical properties in the forward and backward processes we perform isothermal-isobaric Monte Carlo (MC) simulations. More details of the numerical method were presented in [42,43].

For the simulations, Table 1 lists the values of the various parameters in the system. Numerical values are expressed in dimensionless units based on the Lennard-Jones parameters for the solid-solid interaction: distance is expressed in units of σ; energy in units of ϵ_{ss}; stress in units of ϵ_{ss}/σ; temperature in units of ϵ_{ss}/k_B. The film-substrate attractive well depth is supposed to obey a modified combining rule $\epsilon_{fs} = \kappa\sqrt{\epsilon_{ff}\epsilon_{ss}} = \kappa/3$, where κ is an adjustable constant. ϵ_{fs} and ϵ_{ff} represent approximately the adhesion strength between the film and substrates and the cohesive strength of the film in the system, respectively. In the following, we take two cases of (three-layer and four-layer) molecularly thin-film to investigate effects of the film-substrate coupling strength and loads on the tribological dynamical processes of the thin-film lubrication system at fixed ϵ_{ss} and ϵ_{ff}.

3. Results

3.1. Three-layer molecularly thin-film lubrication

3.1.1. Effects of film-substrate coupling strength at a fixed load

Fig. 2 displays plots of the shear stress T_{yx} and the mean separation L_y between walls for the three-layer molecularly thin-film lubrication system at the load $T_{yy} = -1.0$ as a function of register α for different $\kappa(\epsilon_{fs})$. Since all shear-stress and mean separation profiles possess similar behaviors, we take $\kappa = 1$ ($\epsilon_{fs} = 1/3$) as an example to summarize their common features. The profiles display a forward periodic process in α with a period length 1, which composites two elastic (stick) regions ($0 \leqslant \alpha < 0.6, 0.7 < \alpha \leqslant 1$) and a transition (slip) region ($0.6 \leqslant \alpha \leqslant 0.7$). At $\alpha = 0$, fluid atoms with an initial random distribution converge to a stable close-packed structure with solid atoms of the upper and lower substrates as shown in Fig. 3(a). The perfect symmetric atomistic structure exhibits the system in an equilibrium state and leads to $T_{yx,cf} = 0$. As α increases gradually in the range $0 < \alpha < 0.6$, the upper and lower substrates adsorbing the film just like a whole crystal to generate

Table 1
Parameters of the simulation. Reduced dimensionless units are based on the Lennard-Jones parameters (σ, ϵ_{ss}) of the substrate, as explained in text.

Number of fluid atoms for a threelayer film	$N_f = 30$
Number of fluid atoms for a fourlayer film	$N_f = 40$
Number of wall atoms	$N_w = 2\times 40 = 80$
Total number of substrate atoms	$N_s = 2\times 240 = 480$
Number of near-region atoms	$N_s' = 2\times 40 = 80$
Number of far-region atoms	$N_s'' = 2\times 200 = 400$
Number of elements	$N_e = 2\times 4 = 8$
Number of nodes	$N_n = 2\times 2 = 4$
Lattice constant of substrate	$a = \sqrt{\frac{2}{\sqrt{3}}} = 1.075$
Width of contact	$L_x = 10a$
Temperature	$T = 0.1$
Substrate–substrate Lennard-Jones well depth	$\epsilon_{ss} = 1$
Film-film Lennard-Jones well depth	$\epsilon_{ff} = 1/9$
Cutoff radius	$r_c = 2.5$
Total number of Monte Carlo cycles for each α	10^6

an elastic shear behavior in the x direction. The film atoms as in a solid state hold the shear stress in the system. A net force provided to the upper substrate/the film by the film/the lower substrate varies stronger and leads to the increase of $T_{yx,cf}$. Meanwhile, to hold the shear stress in the thin film, the effective film thickness (or the mean separation L_y) also increases. As α varies in the range $0.6 \leqslant \alpha \leqslant 0.7$, the systematic shear strain reaches a critical value, which corresponds to the largest shear stress. For the lubrication system, the interaction between the film and the substrates or among the interlayers in the film cannot hold the strong shear stress. Under the action of the shear stress, the interlayer atoms in the film or the surface atoms of the upper substrate abruptly stride over the atoms in the layer touching with them as barriers, so that the upper and lower substrates make a relative slippage to restrain the increase of the systematic shear stress. After the sliding process, the system performs again an elastic shear behavior. Since the net force provided to the upper substrate/the film by the thin film atoms/the lower substrate has changed its direction, the shear stress is negative. In this process, the effective film thickness (or the mean separation L_y) reaches the largest value and then drops gradually. When α increases continuously in the range $0.7 < \alpha < 1$, the systematic behavior is asymmetric with that at $1 - \alpha$. When the register finally reaches $\alpha = 1$, the system is precisely in the same state as it is at $\alpha = 0$. As α increases from 1 to 1.2, the above profiles in the range $0 < \alpha \leqslant 0.2$ are repeated. Shearing from $\alpha = 1.2$ to $\alpha = 0$ carries the system in reverse through the same states as shearing in the forward direction. In the forward and backward processes, the slip process deviates from the center $\alpha = 0.5$ but appears at its both sides duo to the longer relaxation time required to reach the quasi-equilibrium state [46,47]. So the paths for the stick and the slip processes constitute a hysteresis loop.

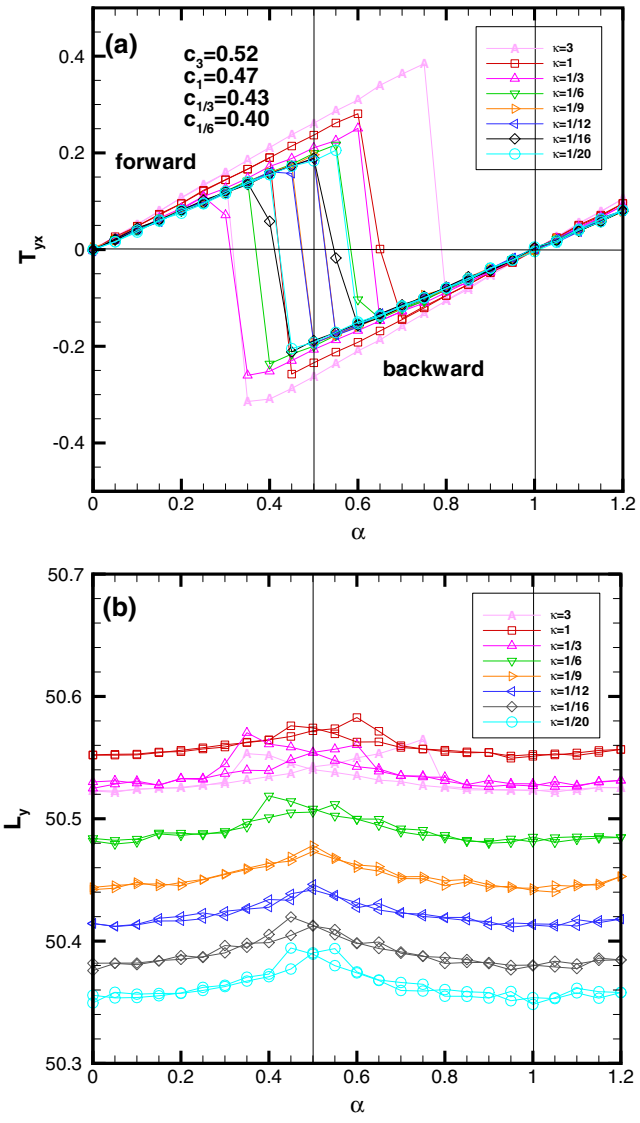

Fig. 2. (a) Shear stress $T_{yx,cf}$ versus register α; (b) mean-separation profile for the coarse-grained 2D model contact with the three-layer thin-film at a fixed load $T_{yy} = -1.0$.

In Fig. 2(a), the thermal elastic coefficient ($c_\kappa = \frac{\Delta T_{yx,cf}}{\Delta \alpha}$) in the stick process decreases when κ decreases from 3 to 1/6. It is almost a constant when κ decreases over $1/6 \leqslant \kappa \leqslant 1/20$. The thermal elastic coefficient reflects the ability of the system resisting the shear strain. The larger $\kappa(\epsilon_{fs})$ has influence on c_κ while the smaller $\kappa(\epsilon_{fs})$ is insensitive to it. So only the larger one between ϵ_{fs} and ϵ_{ff} is more significant to determine the thermal elastic coefficient of the system. Meanwhile, the width of the hysteresis loop reveals the deviation of the system from the quasi-equilibrium state. The larger $\kappa(\epsilon_{fs})$ corresponds to the more width of the hysteresis loop while the smaller $\kappa(\epsilon_{fs})$ is insensitive to it. So the width of hysteresis loop has the above similar features with the thermal elastic coefficient. Moreover, in Fig. 2(b), the mean separation L_y (or the effective film thickness) monotonically decreases with decreasing κ except $\kappa = 3$. In the interaction between the film and the substrates at $\kappa = 3$ ($\epsilon_{fs} = \epsilon_{ss}$), the film atoms adsorbed by the substrates take effects as the surface atoms of the substrates. So the effective film thickness is reduced approximately from three-layer to monolayer. This leads to the decrease of L_y. In order to display the effects of κ on the shearing transitions, three kinds of the atomistic configuration of the film and the near substrates at $\alpha = 0$ and $\alpha = 1.0$ for the different $\kappa(\epsilon_{fs})$ are shown in Fig. 3.

(1) The slip process appearing in the internal layers of the film atoms is termed as the internal slip. (i) For $\kappa = 3$ and 1, ϵ_{fs}(=1 and 1/3) is larger than ϵ_{ff}. In the thin-film lubrication system, the weakest interaction among atoms appears in the film. The slip process happens between the first and second layers in the film as shown in Fig. 3(b). The fluid atoms of the first layer are moved a lattice distance to the right with respect to the second layer in the film. At the same time, the upper substrate adsorbing the fluid atoms of the first layer is moved together with the first layer in the film. (ii) For $\kappa = 1/3, \epsilon_{fs}$(=1/9) is equal to ϵ_{ff}. In the thin-film lubrication system, the weaker interaction of the atoms appears in the film and between the substrates and the film. The slip process happens between the second and the third layers in the film as shown in Fig. 3(c). The fluid atoms of the second layer is moved a lattice distance to the right with respect to the third layer in the film. In this case, the first layer in the film adsorbed by the upper substrate is moved together with the second layer in the film.

(2) The slip process appearing between the film and substrates is termed as the interfacial slip. (iii) For $\kappa = 1/6$ and 1/9, ϵ_{fs}(=1/18 and 1/27) is smaller than ϵ_{ff}. In the thin-film lubrication system, the weakest interaction among atoms appears between the substrates and the film. The slip process happens between the upper substrate and the first layer in the film as shown in Fig. 3(d). The surface atoms of the upper substrate are moved a lattice distance to the right with respect to the first layer in the film. (iv) For $\kappa = 1/12, \epsilon_{fs}$(=1/36) is smaller than ϵ_{ff}. In the thin-film lubrication system, the weakest interaction among atoms also

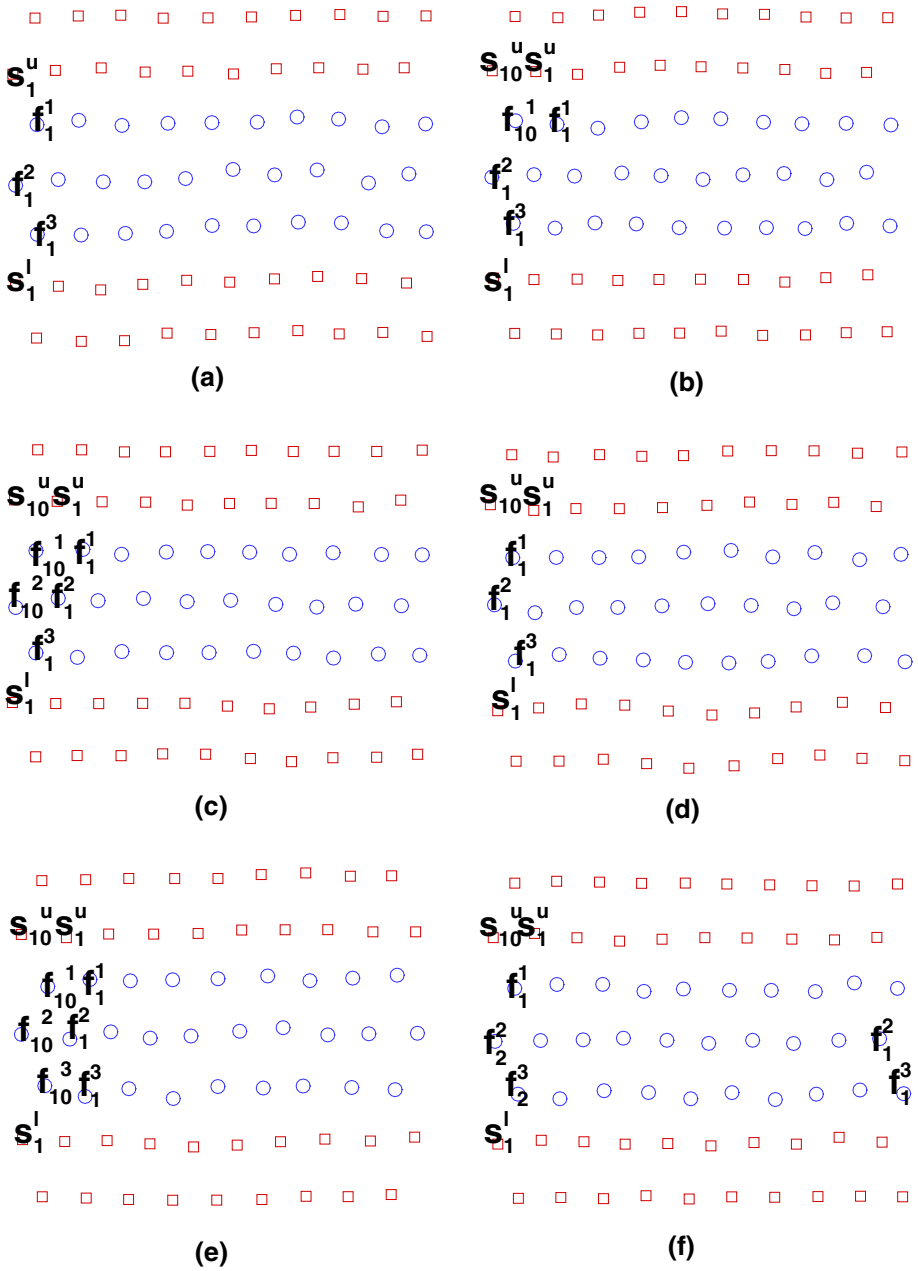

Fig. 3. Atomistic structures of the fluid film and the near substrates at the identical state at $\alpha = 0$ for all κ (a) and the different states at $\alpha = 1.0$ for (b) $\kappa = 1$; (c) 1/3; (d) 1/6; (e) 1/12; (f) 1/16. *f* and *s* denote the fluid atoms in the film and the solid atoms in the substrates, respectively. The superscripts of *f* and *s* denote the layer coding in the film and the upper/lower substrates, respectively. The subscripts of *f* and *s* denote the position coding in a layer at $\alpha = 0$ in Fig. 3(a).

appears between the substrates and the film. The slip process happens between the third layer in the film and the lower substrate as shown in Fig. 3(e). The fluid atoms in the third layer are moved a lattice distance to the right with respect to the lower substrate.

(3) The slip processes appearing not only between the internal layers of the film atoms but also between the film and substrates are termed as the mixing slip, i.e., mixing of the internal and the interfacial slips. (v) For $\kappa = 1/16$ and 1/20, ϵ_{fs}(=1/48 and 1/60) is smaller than ϵ_{ff}. In the thin-film lubrication system, the weakest interaction among atoms appears between the substrates and the film. The slip processes happen simultaneously between the upper substrate and the first layer in the film, between the first and second layers in the film and between the third layer in the film and the lower substrate as shown in Fig. 3(f). Only the second and the third layers in the film move together. The surface atoms in the upper substrate are moved a lattice distance to the right with respect to the first layer in the film. The fluid atoms in the second and third layers are moved a lattice distance to the left with respect to the first layer in the film and the lower substrate.

3.1.2. Effects of loads at a fixed film-substrate coupling strength

Fig. 4 displays the shear-stress and the mean separation profiles of the three-layer molecularly thin-film lubrication at $\kappa = 1$ ($\epsilon_{sf} = 1/3$) for different load $-T_{yy}$ on the system. As the load $-T_{yy}$ increases, the thermal elastic constant c_1 increases and the width of the hysteresis loop enlarges. Meanwhile, the vertical movement of the atoms in the system is more restrained. It leads to the decrease of the effective film thickness (or the mean separation

L_y). For $T_{yy} = -0.5$, the slip process happens between the second and third layers in the film. The fluid atoms of the second layer are moved a lattice distance to the right with respect to those of the third layer. At the same time, the first layer in the film adsorbed by the upper substrate is moved together with the second layer in the film. For $T_{yy} = -1.0$, the slip process happens between the first and second layers in the film. The fluid atoms of the first layer are moved a lattice distance to the right with respect to those of the second layer. For $T_{yy} = -1.5$, the slip process happens between the second and third layers in the film. The fluid atoms of the second layer are moved a lattice distance to the right with respect to those of the third layer. So the internal slip at the fixed $\kappa = 1$ ($\epsilon_{sf} = 1/3$) is kept as the load increases. In comparing with the effects of the film-substrate coupling strength on the system, it is found that the effects of the load $-T_{yy}$ on the system have similar tribological dynamical behaviors (the thermal elastic constant and the width of the hysteresis loop), but are opposite on the effective film thickness (or the mean separation L_y) in system.

3.2. Four-layer molecularly thin-film lubrication

3.2.1. Effects of film-substrate coupling strength at a fixed load

Fig. 5 displays plots of the shear stress T_{yx} and the mean separation L_y for the four-layer molecularly thin-film lubrication system at the load $T_{yy} = -1.0$ as a function of register α for different $\kappa(\epsilon_{fs})$. Since all shear-stress profiles possess similar behaviors, we take $\kappa = 1$ ($\epsilon_{fs} = 1/3$) as an example to summarize their common features. The profiles display a forward periodic process in α with a period length 1. The periodic process composites two elastic (stick) regions ($-0.5 \leqslant \alpha < 0.1, 0.15 < \alpha \leqslant 0.5$) and a transition (slip) region ($0.1 \leqslant \alpha \leqslant 0.15$). At $\alpha = -0.5$, the film atoms with an initial random distribution converge to a stable close-packed structure with the surface atoms of the upper and lower substrates as shown in Fig. 6(a). It exhibits the system in an equilibrium state with $T_{yx,cf} = 0$. As α increases gradually from -0.5 to 0.1, the elastic shear behavior to the x direction in the combination of the upper and lower substrates connected by the film is enhanced. This leads directly to the increase of $T_{yx,cf}$. As α increases in the range $0.1 < \alpha < 0.15$, the fluid atoms in the film abruptly stride over

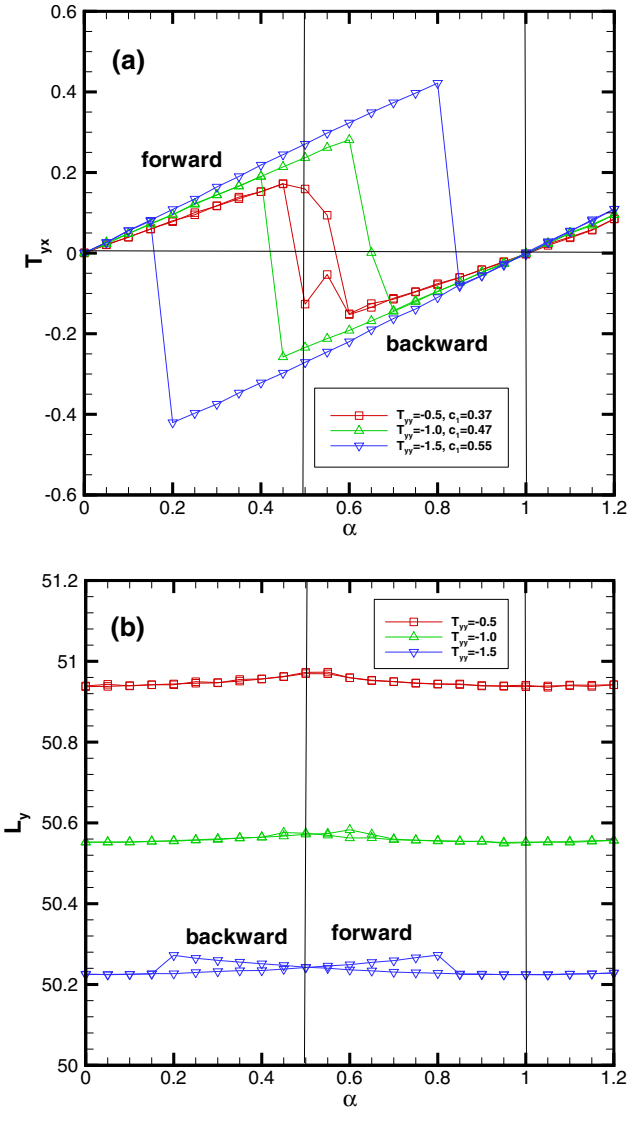

Fig. 4. (a) Shear stress $T_{yx,cf}$ versus register α; (b) mean-separation profile for the coarse-grained 2D model contact with the three-layer thin-film at a fixed $\epsilon_{fs} = 1/3(\kappa = 1)$.

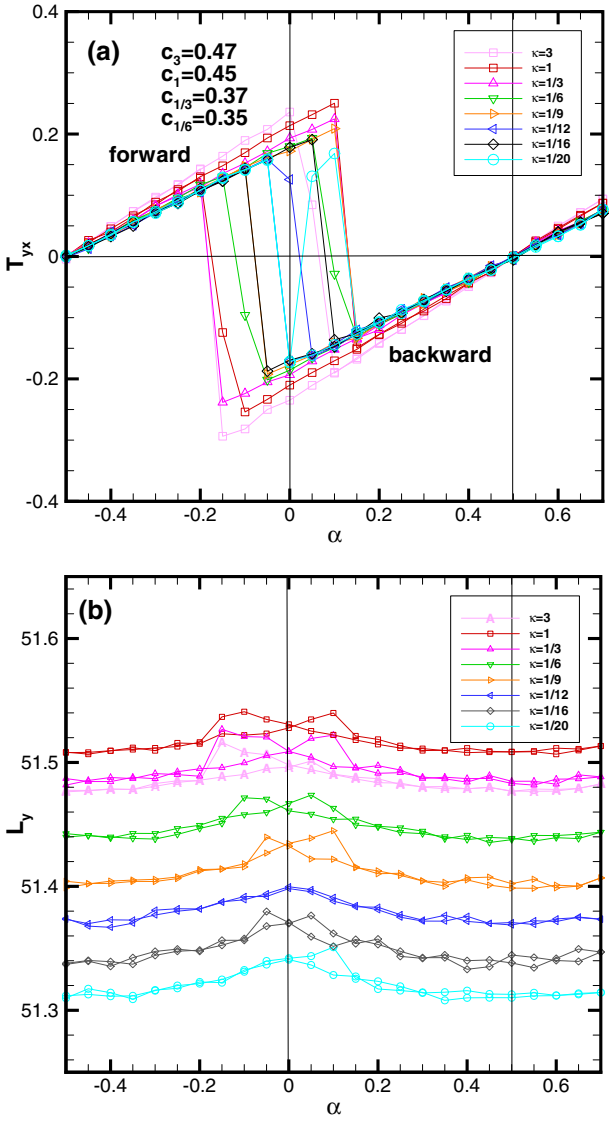

Fig. 5. (a) Shear stress $T_{yx,cf}$ versus register α; (b) mean-separation profile for the coarse-grained 2D model contact with the four-layer thin-film at a fixed load $T_{yy} = -1.0$.

the atoms in the layer touching with them as barriers, so that the shear strain between the upper and lower substrates are varied from a positive value to a negative one. As α increases gradually from 0.15 to 0.5, the systematic behavior is asymmetric with that at $-\alpha$, i.e., the shear strain of the system is varied from the negative value to zero. When the register finally reaches $\alpha = 0.5$, the system is in precisely the same state as it is at $\alpha = -0.5$. As α increases from 0.5 to 0.7, the above scenario ($-0.5 < \alpha < -0.3$) is repeated. Shearing from $\alpha = 0.7$ to $\alpha = -0.5$ carries the system in reverse through precisely the same states as shearing in the forward direction.

In Fig. 5, the thermal elastic coefficient c_κ decreases when κ decreases from 3 to 1/6. It is almost a constant when κ decreases over $1/6 \leqslant \kappa \leqslant 1/20$. Meanwhile, as $\kappa(\epsilon_{fs})$ decreases, the width of hysteresis loop has the above similar features with the thermal elastic coefficient. Moreover, the mean separation L_y (or effective film thickness) monotonically decreases with decreasing κ except $\kappa = 3$. In the interaction between the film and the substrates at $\kappa = 3$ ($\epsilon_{fs} = \epsilon_{ss}$), the film atoms adsorbed by the substrates take effects as the surface atoms of the substrates, so that the effective film thickness is reduced approximately from four-layer to two-layer. This leads to the decrease of L_y. In order to display the effects of κ on the shearing transitions, two kinds of the atomistic configuration of the film and the near substrates at $\alpha = -0.5$ and $\alpha = 0.5$ for the different ϵ_{fs} are shown in Fig. 6.

(1) The internal slip: (i) for $\kappa = 3$, 1 and 1/3, ϵ_{fs}(=1, 1/3 and 1/9) is not smaller than ϵ_{ff}. The slip process happens between the second and third layers in the film as shown in Fig. 6(b). The fluid atoms of the second layer are moved a lattice distance to the right with respect to those of the third layer. In this case, the first layer in the film adsorbed by the upper substrate is moved together with the second layer in the film. (ii) For $\kappa = 1/6$, ϵ_{fs}(=1/18) is smaller than ϵ_{ff}. The slip process happens between the third and fourth layers in the film as shown in Fig. 6(c). The fluid atoms of the third layer is moved a lattice distance to the right with respect to those of the fourth layer. At the same time, the second layer in the film is moved together with the third layer in the film.

(2) The interfacial slip: (iii) for $\kappa = 1/9$ and 1/12, ϵ_{fs}(=1/27 and 1/36) is smaller than ϵ_{ff}. The slip process happens between the upper substrate and the first layer in the film as shown in Fig. 6

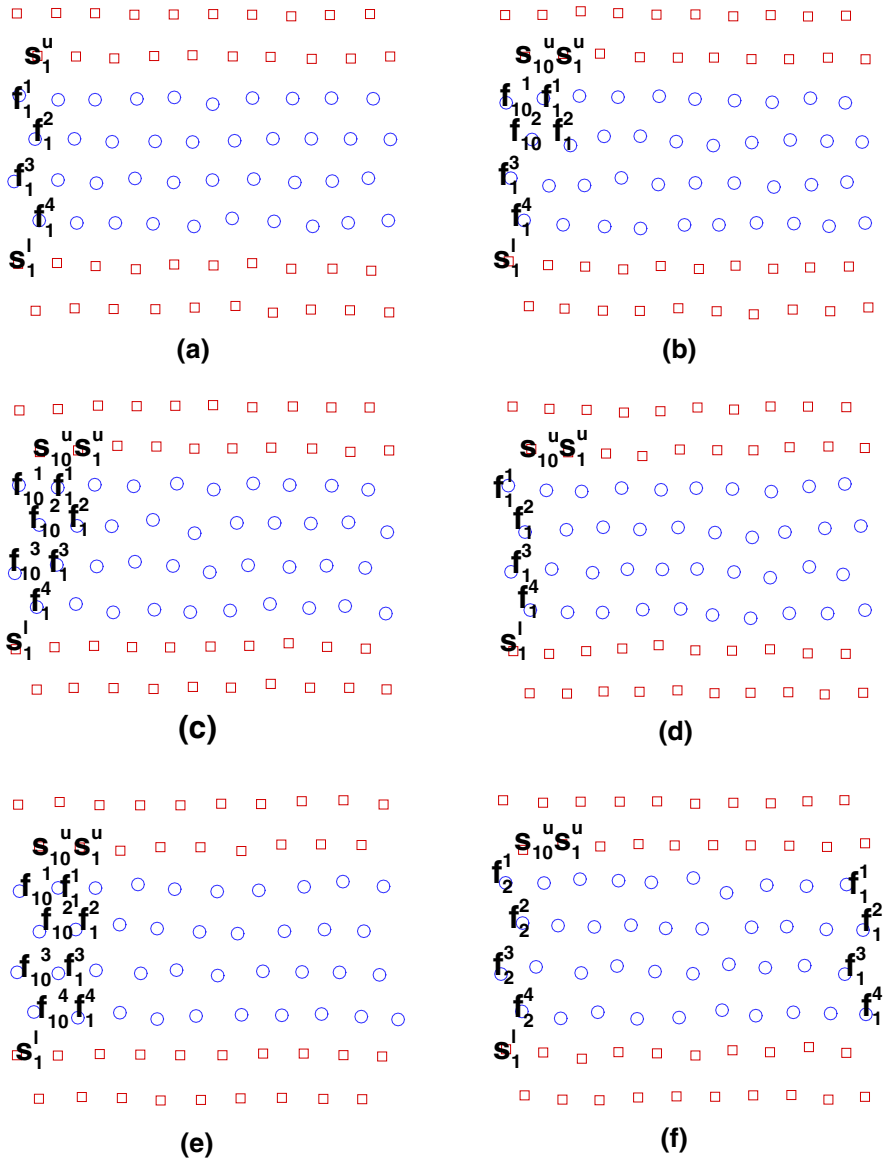

Fig. 6. Atomistic structures of the fluid films and the near substrates at the identical state at $\alpha = -0.5$ for all κ (a) and the different states at $\alpha = 0.5$ for (b) $\kappa = 1$; (c) 1/6; (d) 1/9; (e) 1/12; (f) 1/20. Notation as in Fig. 3.

(d). The surface atoms of the upper substrate are moved a lattice distance to the right with respect to the first layer in the film. (iv) For $\kappa = 1/12$ and 1/16, ϵ_{fs}(=1/36 and 1/48) is smaller than ϵ_{ff}, the slip process happens between fourth layer in the film and the lower substrate as shown in Fig. 6(e). The fluid atoms in the fourth layer are moved a lattice distance to the right with respect to to the lower substrate.

(3) The slip processes appearing not only between the film and the upper substrate but also between the film and the lower substrate are also termed as the mixing slip, i.e., mixing of the upper and lower the interfacial slips. (v) For $\kappa = 1/20, \epsilon_{fs}$(=1/60) is smaller than ϵ_{ff}. The slip processes appear not only between the upper substrate and the first layer in the film but also between the fourth layer in the film and the lower substrate as shown in Fig. 6(f). The fluid atoms of the first, second, third and fourth layers are moved a lattice distance to the right with respect to the lower substrate. The surface atoms of the upper substrate are moved two lattice distance to the right with respect to the first layer in the film. So the upper and lower substrates have only the relative slippage with a lattice distance.

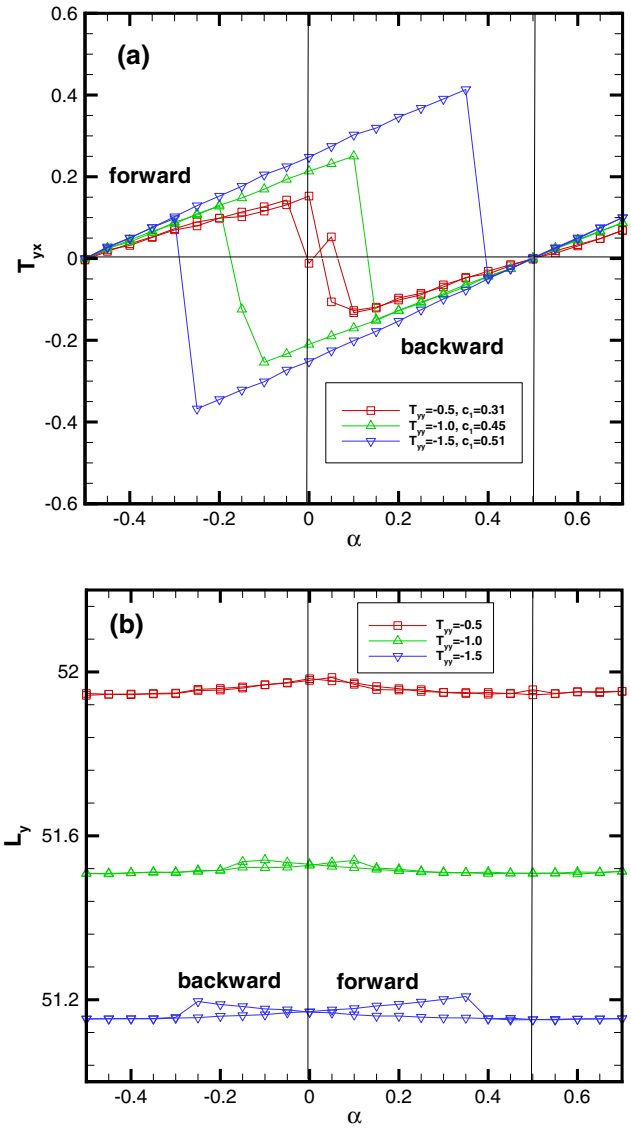

Fig. 7. (a) Shear stress $T_{yx.cf}$ versus register α; (b) mean-separation profile for the coarse-grained 2D model contact with the four-layer thin-film at a fixed $\epsilon_{fs} = 1/3(\kappa = 1)$.

3.2.2. Effects of loads at a fixed film-substrate coupling strength

Fig. 7 displays the shear-stress and the mean separation profiles of the four-layer molecularly thin-film lubrication at $\kappa = 1$ ($\epsilon_{sf} = 1/3$) for different load $-T_{yy}$ on the system. As the load $-T_{yy}$ increases, the thermal elastic constant increases and the width of the hysteresis loop enlarges. Meanwhile, L_y (or the effective film thickness) becomes thinner. For $T_{yy} = -0.5$, the slip processes happen not only between the first and second layers, between the second and third atomistic layers in the film, but also between the third and fourth layers in the film. The fluid atoms of the third layer are moved a lattice distance to the right with respect to those of the fourth layer. The fluid atoms of the second layer are moved a lattice distance to the right with respect to those of the third layer. The fluid atoms of the first layer are moved a lattice distance to the left with respect to those of the second layer. So the surface atoms of the upper substrate and the fluid atoms of the first layer are moved together a lattice distance to the right with respect to those of the fourth layer adsorbed by the lower substrate. The slip processes with the multiple internal slips are also termed as the mixing slip. For $T_{yy} = -1.0$, the slip process happens between the second and third layers in the film. The fluid atoms of the second layer are moved a lattice distance to the right with respect to those of the third layer. For $T_{yy} = -1.5$, the slip process happens between the third and fourth layers in the film. The fluid atoms of the third layer are moved a lattice distance to the right with respect to those of the fourth layer. So in the four-layer thin-film lubrication at the fixed $\kappa = 1$ ($\epsilon_{sf} = 1/3$), the mixing slip is changed to the internal slip as the load increases. In comparing with the effects of the film-substrate coupling strength on the system, it is found that the effects of the load $-T_{yy}$ on the system have similar tribological dynamical behaviors (the thermal elastic constant and the width of the hysteresis loop), but are opposite on the effective film thickness (or the mean separation L_y) in system.

4. Conclusions and discussions

Shearing transitions of multi-layer molecularly film lubrication systems in variations of the film-substrate coupling strength and the load have been studied by using a hybrid atomistic-coarse-grained method. For the thin-film lubrication with multi-layer molecules at a fixed load, three kinds of the interlayer slips (the internal, the interfacial and the mixing slips) in the system are found as the film-substrate coupling strength decreases. The internal and the interfacial slips have one relative slippage in the interlayers of the systems, but the mixing slip has more relative slippages in them. For the three-layer molecularly thin-film lubrication, the mixing slip includes the internal slip and the upper and lower interfacial slips. For the four-layer molecularly thin-film lubrication, the mixing slip includes the upper and lower interfacial slips or the multiple internal slips. These phenomena are in qualitative agreement with the experimental results [8,9]. Meanwhile, the tribological dynamical behaviors (the thermal elastic constant and the width of the hysteresis loop) are almost insensitive to the smaller film-substrate coupling strength. However, they and the effective film thickness are enlarged more and more as the larger film-substrate coupling strength increases. When the load increases, the tribological dynamical behaviors are similar to those in increasing film-substrate coupling strength, but the effective film thickness is opposite.

Acknowledgments

This research is supported by the National Natural Science Foundation of China through the Grants No. 11172310 and No. 11472284, and the CAS Strategic Priority Research Program

XDB22040403. The author thanks the IMECH research computing facility for assisting in the computation.

References

[1] A.W. Adamson, A.P. Gast, Physical Chemistry of Surfaces, sixth ed., Wiley, New York, 1997.
[2] M. Scherge, S.S. Gord, Biological Mirco- and Nanotribology, Springer, Berlin, 2001.
[3] M. Nosonovsky, B. Bhushan, Multiscale Dissipative Mechanisms and Hierarchical Surfaces, Springer, Berlin, 2008.
[4] J.N. Israelachvili, P.M. McGuiggan, A.M. Homola, Dynamic properties of molecularly thin liquid films, Science 240 (1988) 189–191.
[5] J.V. Alsten, S. Granick, Molecular tribometry of ultrathin liquid films, Phys. Rev. Lett. 61 (1988) 2570–2573.
[6] M. Schoen, C.L. Rhykerd, D.J. Diestler, J.H. Cushman, Shear forces in molecularly thin films, Science 245 (1989) 1223–1225.
[7] D.J. Diestler, M. Schoen, J.H. Cushman, On the thermodynamic stability of confined thin films under shear, Science 262 (1993) 545–547.
[8] J.N. Israelachvili, Intermolecular and Surface Force, third ed., Academic Press, New York, 2011, pp. 486–487.
[9] S. Yamada, Nanotribology of symmetric and asymmetric liquid lubricants, Symmetry 2 (2010) 320–345.
[10] J. Jiang, R.D. Arnell, J. Tong, The effect of substrate properties on tribological behaviur of composite DLC coatings, Tribol. Inter. 30 (1997) 613–625.
[11] J.M. Jungk, J.R. Micheal, S.V. Prasad, The role of substrate plasticity on the tribological behavior of diamond-like nanocomposite coatings, Acta Meta. 56 (2008) 1956–1966.
[12] X. Wu, T. Ohana, T. Nakamura, A. Tanaka, Hardness effect of stainless steel substrates on tribological properties of water-lubricated DLC films against AISI 440C ball, Wear 268 (2010) 329–334.
[13] S. Kohlhoff, P. Gumbsch, H.F. Fischmeister, Crack propagation in b.c.c crystals studies with a combined finite-element and atomistic model, Philos. Mag. A 64 (1991) 851–878.
[14] E.B. Tadmor, M. Ortiz, R. Phillips, Quasicontinuum analysis of defects in solids, Philos. Mag. A 73 (1996) 1529–1563.
[15] V. Shenoy, V. Shenoy, R. Phillips, Finite temperature quasicontinuum methods, Mater. Res. Soc. Sym. Proc. 538 (1999) 465–471.
[16] J.Q. Broughton, F.F. Abraham, N. Bernstein, E. Kaxiras, Concurrent coupling of length scales: methodology and application, Phys. Rev. B 60 (1999) 2391–2403.
[17] R.E. Rudd, J.Q. Broughton, Concurrent coupling of length scales in solid state systems, Phys. Status Solidi (b) 217 (2000) 251–291.
[18] M. Ortiz, A.M. Cuitino, J. Knap, M. Koslowski, Mixed atomistic continuum models of material behavior: the art of transcending atomistics and informing continua, MRS Bull. 26 (2001) 216–221.
[19] R.E. Miller, E.B. Tadmor, The quasicontinuum method: overview, applications and current directions, J. Comput.-Aid. Mater. Des. 9 (2002) 206–239.
[20] R.M. Nieminen, From atomistic simulation towards multiscale modelling of materials, J. Phys.: Condens. Matter 14 (2002) 2859–2876.
[21] R. Phillips, M. Dittrich, K. Schulten, Quasicontinuum representations of atomic-scale mechanics: from proteins to dislocations, Annu. Rev. Mater. Res. 32 (2002) 219–233.
[22] Z.B. Wu, D.J. Diestler, R. Feng, X.C. Zeng, Coarse-graining description of solid systems at nonzero temperature, J. Chem. Phys. 119 (2003) 8013–8023.
[23] D.J. Diestler, Z.-B. Wu, X.C. Zeng, An extension of the quasicontinuum treatment of multiscale solid systems to nonzero temperature, J. Chem. Phys. 121 (2004) 9279–9282.
[24] M. Fago, R.L. Hayes, E.A. Carter, M. Ortiz, Density-functional-theory-based local quasicontinuum method: prediction of dislocation nucleation, Phys. Rev. B 70 (2004) 100102.
[25] R.E. Rudd, J.Q. Broughton, Coarse-grained molecular dynamics: nonlinear finite elements and finite temperature, Phys. Rev. B 72 (2005) 144104.
[26] S.P. Xiao, W.X. Yang, Temperature-related Cauchy-Born rule for multiscale modeling of crystalline solids, Comput. Mater. Sci. 37 (2006) 374–379.
[27] V. Gavini, K. Bhattacharya, M. Ortiz, Quasi-continuum orbital-free density-functional theory: a route to multi-million atom non-periodic DFT calculation, J. Mech. Phys. Solids 55 (2007) 697–718.
[28] D. Negrut, M. Anitescu, A. El-Azab, P. Zapol, Quasicontinuum-like reduction of density functional theory calculations of nanostructures, J. Nanosci. Nanotech. 8 (2008) 3729–3740.
[29] N. Bernstein, J.R. Kermode, G. Csanyi, Hybrid atomistic simulation methods for materials systems, Rep. Prog. Phys. 72 (2009) 026501.
[30] J. Marian, G. Venturini, B.L. Hansen, J. Knap, M. Ortiz, G.H. Campbell, Finite-temperature extension of the quasicontinuum method using Langevin dynamics: entropy losses and analysis of errors, Model. Simul. Mater. Sci. Eng. 18 (2010) 015003.
[31] M. Iyer, V. Gavini, A field theoretical approach to the quasi-continuum method, J. Mech. Phys. Solids 59 (2011) 1506–1535.
[32] X.H. Li, M. Luskin, C. Ortner, Positive definiteness of the blended force-based quasicontinuum method, Multiscale Model. Simul. 10 (2012) 1023–1045.
[33] E.B. Tadmor, F. Legoll, W.K. Kim, L.M. Dupuy, R.E. Miller, Finite-temperature quasi-continuum, Appl. Mech. Rev. 65 (2013) 010803.
[34] W.K. Kim, M. Luskin, D. Perez, A.F. Voter, E.B. Tadmor, Hyper-QC: an accelerated finite-temperature quasicontinuum method using hyperdynamics, J. Mech. Phys. Solids 63 (2014) 94–112.
[35] J.S. Amelang, G.N. Venturini, D.M. Kochmann, Summation rules for a fully-nonlocal energy-based quasicontinuum method, J. Mech. Phys. Solids 82 (2015) 378–413.
[36] W.G. Noid et al., The multiscale coarse-graining method. I. A rigorous bridge between atomistic and coarse-grained models, J. Chme. Phys. 128 (2008) 244114.
[37] W.G. Noid et al., The multiscale coarse-grainning method. II. Numerical implementation for coarse-grained molecular models, J. Chem. Phys. 128 (2008) 244115.
[38] P. Sherwood, B.R. Brooks, M.S. Sansom, Multiscale methods for macromolecular simulations, Curr. Opin. Struct. Biol. 18 (2008) 630.
[39] H.L. Woodcock, B.T. Miller, M. Hodoscek, A. Okur, J.D. Larkin, J.W. Ponder, B.R. Brooks, MSCALE: a general unility for multiscale modeling, J. Chem. Theory Comput. 7 (2011) 1208.
[40] A. Singharoy, A.M. Yesnik, P. Ortoleva, Multiscale analytic continuation approach to nanosystem simulation: application to virus electrostatics, J. Chem. Phys. 132 (2010) 174112.
[41] A. Singharoy, H. Joshi, P.J. Ortoleva, Multiscale macromolecular simulation: role of evolving ensembles, J. Chem. Inf. Model. 52 (2012) 2638–2649.
[42] Z.-B. Wu, D.J. Diestler, X.C. Zeng, Multiscale simulation of thin-film lubrication, Mol. Simul. 31 (2005) 811–815.
[43] Z.-B. Wu, X.C. Zeng, Multiscale simulation of thin-film lubrication: free-energy corrected coarse graning, Phys. Rev. E 90 (2014) 033303.
[44] O.M. Braun, M. Paliy, S. Consta, Ordering of a thin lubricant film due to sliding, Phys. Rev. Lett. 92 (2004) 256103.
[45] R. LeSar, R. Najafabadi, D.J. Srolovitz, Finite-temperature defect properties from free-energy minimization, Phys. Rev. Lett. 63 (1989) 624–627.
[46] D.J. Diestler, G.T. Gao, X.C. Zeng, Role of hyperesis in the molecular picutre of friction, Phys. Chem. Chem. Phys. 3 (2001) 1175–1178.
[47] D.J. Diestler, Constranied statistical thermodynamic treatment of friction, J. Chem. Phys. 117 (2002) 3411–3424.